iomac
International Operational Modal Analysis Conference
11th International Operational Modal Analysis Conference
20 - 23 May 2025 | Rennes, France

1D-CAE model building and simulation based on modal parameter identification of Electrical-Mechanical coupling system

Soichiro Takata[1]

[1] National Institute of Technology, Tokyo College, takata@tokyo-ct.ac.jp

ABSTRACT

Infrastructure sensing instruments are well-developed in many fields; however, existing measurement devices mainly use passive sensing methods. The vibration response from infrastructure is fundamental small because of its static structure. Thus, the modal response could not be sufficiently measured using microtremors. This study develops a vibration-active sensing device to detect infrastructure deterioration. Previous active sensing methods mainly used scientific measurement instruments, and structural monitoring using these methods is limited. Thus our development target was a simplified active sensing device composed of an Internet of Things sensor and device. Our active vibration-sensing device contained an electrodynamic vibration speaker to excite the target vibration mode. Thus, the desired vibrational mode can be selectively excited in the principal subcomponent, or component structures. Therefore, the device can sufficiently obtain the desired modal response. In development, the most important aspect is the systematic analysis of the electro-dynamic speaker and structure. The electro-dynamic speaker has its resonance characteristics (electrical circuit and mechanical resonances), which are affected by the structural resonance characteristics. For a more detailed analysis, an electrical-mechanical coupling analysis is an effective method. Recently, 1D-computer-aided engineering (CAE) has been used to simulate and design multi-physics, multi-domain, and large-degree-of-freedom systems. This study focuses on the 1D-CAE technology. The application to an electrodynamic vibration speaker system (i.e., a typical electrical-mechanical coupling system) was considered. In particular, electrical power consumption was considered. First, a low-dimensional model of an electrical dynamic vibration speaker was derived using 1D-CAE. We determined the frequency-response function of the electro-dynamic vibration speaker based on the measurements of the input voltage and output acceleration. The frequency-response function contains distinct resonance peaks. Moreover, modal parameter identification equations were derived based on governing equation of the electrical-mechanical coupling system and parameteric fitting was performed. Consequently, we obtained reasonable identified values. Additionally, the 1D-CAE simulations were performed using the identified parameters. 1D-CAE simulations were used to calculate the state variables in all terminals. Thus, electrical power consumption was estimated using the source voltage and current.

Keywords: 1D-CAE, System identification, Electrical-mechanical coupling system, Active sensing

1. INTRODUCTION

Infrastructure sensing instruments are well developed in many fields [1-5]. This sensing method is based on physicaly intensive properties; however, existing measurement devices primaly use passive sensing methods. Active sensing methods primaly use scientific measurement specifications; however structural monitoring using these methods is limited. The vibration response from infrastructure is fundamental small because of its static structure. Thus, the modal response could not be sufficiently measured by using microtremors. Typically, the operational modal analysis method uses only the seismometer's response. However, there is a problem of decreased accuracy in situations with a low signal-to-noise ratio and large damping. This study is develops a vibration-active sensing device for the detection of infrastructure deterioration [6-8]. The active vibration-sensing device contained an electrodynamic vibration speaker to excite the target vibration mode. Thus, the desired vibrational mode can be selectively excited in the principal subcomponent, or component structures and can obtain the desired modal response [9-11]. On the other hand, the previous active sensing device was well used by the PZT transducer, the sampling frequency becomes the high sampling rate. Thus, the measurement unit is required as an expensive instrument. Our proposed method has cost merit because the system was composed of the generally used electrodynamic speaker and measurement instrument [12-13].

In device development, the most important task is the systematic analysis of the electro dynamic speaker and structure. The electro-dynamic speaker has its own resonance characteristics (electrical circuit resonance and mechanical resonance), which are affected by the structural resonance characteristics. For a more detailed analysis, an electrical-mechanical coupling analysis is an effective method.

Recently, 1D-computer-aided engineering (CAE) was used to simulate and design multi-physics, multi-domain, and large-degree-of-freedom systems [14-17]. Therefore, the 1D-CAE is suitable for the simulation and state estimation of an electro-dynamic vibration speaker. This study focuses on the 1D-CAE technology. The application to an electrodynamic vibration speaker system (i.e., a typical electrical-mechanical coupling system) was considered with emphasis on electrical power consumption.

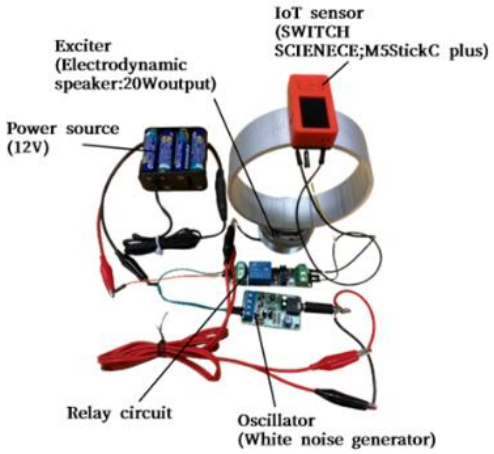

Figure 1. Prototype of vibration sensing actuation device. The device includes the Internet of Things (IoT) sensor, relay circuit, white noise generator, and electro-dynamic speaker.

First, a low-dimensional model of an electrical dynamic vibration speaker was constructed using a 1D-CAE tool. Furthermore, we measured the frequency-response function of the electrodynamic vibration speaker based on input voltage and output acceleration. The frequency-response function exhibited clear resonance peaks. Moreover, modal parameter identification equations were derived based on the

direct current (DC) relationship of the governmening equation of the electrical-mechanical coupling system, and parameteric fitting was performed. Consequently, we obtained reasonable identified values. Additionaly, the 1D-CAE simulations were performed using the identified parameters. 1D-CAE simulations were useed to the state variables in all terminals. Thus, electrical power consumption was estimated using the source voltage and current.

2. THEORETICAL FORMULATION

2.1. 1D-CAE model

In this section, we introduce the 1D-CAE models of an electro-dynamic speaker to activate excitation. The 1D-CAE models are illustrated in **Figure 2**. The model schematics were generated using the OpenModelica software program. The systems are composed of an electrical source, electrical load (i.e., electrical components), an electrical-mechanical transducer, and a mechanical load (i.e., mechanical component). Model (a) considers the electrical resistance, electrical-mechanical transducer, and mechanical stiffness. The model represents the features of the frequency-response function in the low-frequency band. Model (b) is composed of the electrical resistance, electrical-mechanical transducer, mechanical stiffness, mechanical damper, and mechanical mass. This model considers the contribution of the mechanical resonance characteristics of the electrodynamic speaker. Model (c) considers the inductor in Model (b). The model assumes the contribution of the electrical load to the mechanical resonance characteristics of the electrodynamic speaker. This study verified the frequency-response function of each model.

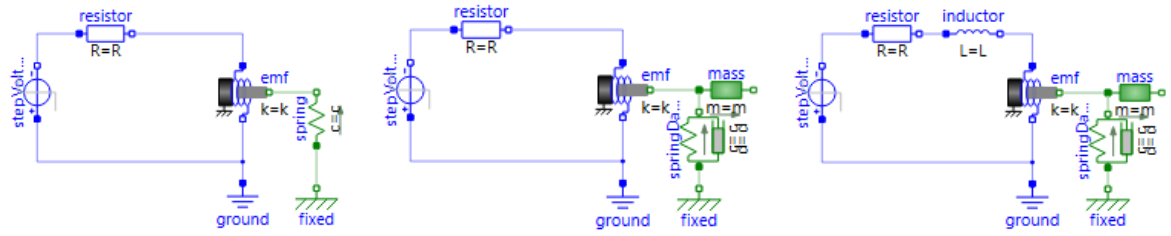

(a) Without mass and inductor (b) Without inductor (c) Full model

Figure 2. Electrical-mechanical coupled system for excitation function in vibration-sensing-actuation device. The schematics were generated using the OpenModelica software program.

2.2. Governing equation

This section describes the governing equations. First, we consider the model shown in **Figure 2** (a). The governing equations were derived from the electrical circuit equation and equilibrium of force in the mechanical system. The governing equation becomes a coupled equation: The electrical equation obeys Ohm' law; thus, the input voltage e_d to the system is equal to the product of the current i_d and the resistance R_d. Additionally, the force equilibrium obeys action-reaction law, and the stiffness reaction force $k_f x_f$ is equal to the generative force Ai_d by the electro-mechanical transducer. Herein, the spring constant is k_f, displacement of the electrodynamic speaker is x_f, and force factor is A. Thus, the governing equation of the circuit in **Figure 2** (a) is Eq. (1).

$$\begin{cases} R_d i_d = e_d \\ k_f x_t = A i_d \end{cases} \tag{1}$$

The frequency-response function of Eq. (1) can be rewritten as Eq. (2). The frequency response was obtained from the ratio between the input voltage and the output acceleration.

$$\frac{\ddot{X}_t(\omega)}{E_d(\omega)} = -\frac{A\omega^2/R_d}{k_f} \tag{2}$$

In this section, we consider the model shown in **Figure 2** (b). Governing equations were derived from the electrical circuit equation and equation of motion in the mechanical system. The circuit equation is the same as Eq. (1). The equation for the mechanical system is expanded using the inertial and damping forces. The governing equation of the circuit shown in **Figure 2** (b) is give by Eq. (3). Herein, the damping constant is r_f, velocity of the electrodynamic speaker is dx_f/dt, mass is m_t, and the acceleration of the electrodynamic speaker is d^2x_f/dt^2.

$$\begin{cases} R_d i_d = e_d \\ m_t \dfrac{d^2x_t}{dt^2} + r_f \dfrac{dx_t}{dt} + k_f x_t = A i_d \end{cases} \tag{3}$$

The frequency-response function of Eq. (3) can be rewritten as Eq. (4). The frequency response was obtained from the ratio between the input voltage and the output acceleration.

$$\frac{\ddot{X}_t(\omega)}{E_d(\omega)} = -\frac{A\omega^2/R_d}{-m_t\omega^2 + k_f + ir_f\omega} \tag{4}$$

We consider the model shown in **Figure 2** (c). Governing equations were derived from the electrical circuit equation and equation of motion in the mechanical system. Herein, the circuit equation is expanded using the voltage by the force factor and the voltage by the inductance. The governing equation of the circuit depicted in **Figure 2** (c) is Eq. (5), where L_d is the inductance.

$$\begin{cases} A\dfrac{dx_t}{dt} + L_d\dfrac{di_d}{dt} + R_d i_d = e_d \\ m_t \dfrac{d^2x_t}{dt^2} + r_f \dfrac{dx_t}{dt} + k_f x_t = A i_d \end{cases} \tag{5}$$

The frequency-response function of Eq. (5) can be rewritten as Eq. (6). The frequency response was obtained from the ratio between the input voltage and the output acceleration.

$$\frac{\ddot{X}_t(\omega)}{E_d(\omega)} = \frac{A\omega^2}{-j\omega A^2 - (j\omega L_d + R_d)\left(-m_t\omega^2 + k_f + ir_f\omega\right)} \tag{6}$$

2.3. Identification method

In this section, the explanation of the identification method is provided using the paradigm of the case presented in **Figure 2** (c). First, the electrical resistance $\hat{R}_d$ was obtained based on direct measurements using an analog multimeter. Furthermore, the spring constant $\hat{k}_f$ and force factor $\hat{A}$ were obtained from the DC relationship (see, Eq. (1)). A fitting analysis was performed using Eq. (2) using the experimental data in the low-frequency band and eigen-frequency f_1. Moreover, the mass was obtained from the mechanical resonant frequency f_0, and the damping constant $\hat{r}_f$ was obtained using the half-power method. Finally, inductance $\hat{L}_d$ is obtained from the following eigen-frequency f_2:

$$f_2 = \frac{1}{2\pi}\frac{\hat{A}}{\sqrt{\hat{m}_t L_d}}. \tag{7}$$

3. EXPERIMENTS

3.1. Frequency-response function measurements

The frequency response was measured using a fast Fourier transform (FFT) analyzer (Ono Sokki, DS-2000). The input-swept sine voltage was generated by the signal output function of the FFT analyzer, and the response was measured using an acceleration pick-up (Ono Sokki, NP-3211). The measurement

conditions were as follows: the sampling frequency was 25.6 kHz, and the voltage ranges were 1.41 V (input voltage) and 0.141 V (response acceleration). The frequency-response functions are shown in **Figure 3**. **Figure 3** (a) shows the frequency responses plotted on logarithmic scales, and **Figure 3** (b) shows the corresponding responses plotted on linear scales. The obtained eigen-frequencies were the f_0 = 300 Hz, f_1 = 100 Hz, and f_2 = 480 Hz.

3.2. Identification results

The identified parameters are listed in **Table 1**. These parameters agree with physical sensations. The fitted results of the frequency-response function are shown in **Figure 4** using the fitted parameters and each supposed model are shown in **Figure 4**. Herein, the blue circle shows the experimental values and the black-dotted line shows the case of Eq. (2) (that is, the model in **Figure 2** (a)), the red-dotted line represents Eq. (4) (that is, the model in **Figure 2** (b)), and the blue-dotted line represents Eq. (6) (the model shown in **Figure 2** (c)). The results of the model shown in **Figures 2** (a) and **2** (b) agree well with the experimental results in the low-frequency band at 100 Hz. In addition, the results of the model shown in **Figure 2** (b) are in good agreement with the mechanical resonance curve at approximately 300 Hz. The results of the model shown in **Figure 2** (c) agree with the inductance resonance curve at approximately 480 Hz.

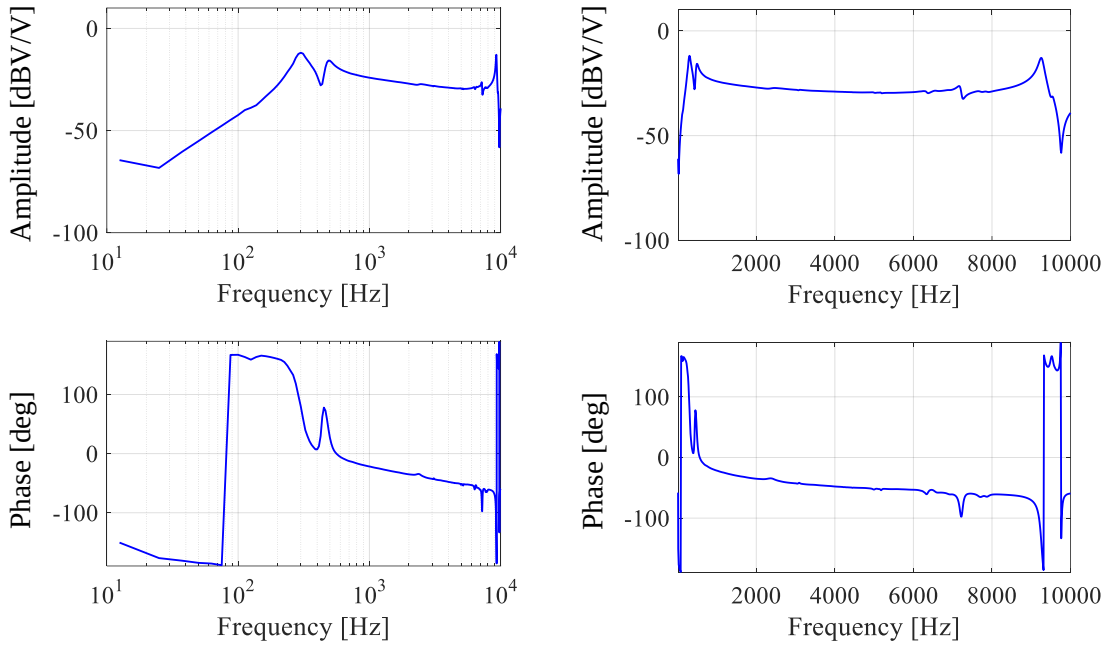

Figure 3. Measured frequency responses (Bode diagrams). The subfigures on the top represent the amplitude (output acceleration divided by the input voltage), and the subfigure on the bottom represent phase differences.

Table 1. Summary of the identified parameters

Variable	R_d[Ω]	L_d[H]	A[N/A]	m_t[kg]	k_f[N/m]	r_f[Ns/m]
Value	4	0.0028	117.8089	0.6136	2.1801×10^6	242.8812

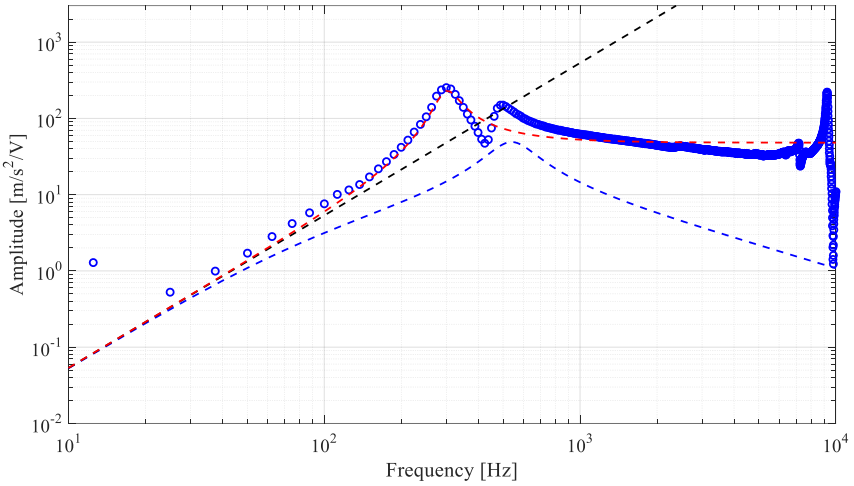

Figure 4. Identification result comparisons between Fig. 2 (a) (without mass and inductor), Fig. 2 (b) (without inductor), and Fig. 2 (c) (full model).

4. SIMULATIONS

This section describes the estimation results of electrical power consumption using the 1D-CAE model which are supposed to be the identified parameters in the previous section. The calculation conditions were as follows: the simulation algorithm was Runge-Kutta, the input voltage signal type was white-noise, the standard deviation of the input white noise is 1, and the discrete-time step was 0.0001 s (i.e., the sampling frequency was 10 kHz).

The calculation results are listed in **Table 2**. The current consumptions were also calculated. The maximum current consumption in shown in **Figure 2** (b). The minimum current consumption in shown in **Figure 2** (c). This implies that these results represent the area under the frequency-response function (i.e., the mean-square value of the response spectrum under whitenoise excitation conditions).

In case the model shown in **Figure 2** (b), the frequency-response function has a constant gain amplitude over the mechanical resonance frequency in the frequency band. Consequently, the current consumption was estimated to be large. In contrast, in the model shown in **Figure 2** (c), the amplitude of the frequency-response function decreased in the frequency region above the mechanical resonance frequency. Thus, the current consumption was estimated to be small.

Table 2. Summary of the estimated results of consumption current

Model	Estimation result of comsumption current	
	Standard deviation [A]	Variance [A^2]
Fig. 2 (a)	0.0430	0.0019
Fig. 2 (b)	0.0595	0.2737
Fig. 2 (c)	0.0035	0.00001

5. CONCLUSIONS

In this paper, we discussed the 1D-CAE model construction and simulations based on the modal parameter identification of an Electrical-mechanical coupling system. The following results were obtained:

(1) The simplified 1D model of an electrical, dynamic vibration speaker was built using a 1D-CAE tool. The simplified model comprised an electrical resistance, inductor, electro-mechanical transduser, a mechanical mass, a spring, and a damper. We considered three types of models (without mass and inductor, without inductor, and with full model).
(2) An identification algorithm was constructed using the governing equations of a simplified 1D-model. The obtained parameters were in agreement with the physical sensation.
(3) Frequency-response function simulations were conducted using the identified parameters. Consequently, the identified frequency-response functions are in good agreement with the experimental values in the case which did not include the inductor model.
(4) A comparison of the estimation of the consumption current was conducted for the three types of models. Consequently, the maximum consumption current was obtained without the inductor model.

ACKNOWLEDGEMENTS

This work was supported by JST Grant Number JPMJPF2115.

REFERENCES

[1] V. Q. C. Tran, D. V. Le, D. R. Yntema, and J. M. Havinga, A review of inspection methods for continuously monitoring PVC drinking water mains, *IEEE Internet of Things Journal*, 9(16), DOI:10.1109/JIOT.2021.3077246, 2022.

[2] Z. He, W. Li, H. Salehi, H. Zhang, H. Zhou, and P. Jiao, Integrated structural health monitoring in bridge engineering, *Automation in construction*, 136, 104168, DOI: 10.1016/j.autcon.2022.104168, 2022.

[3] S. Sattar, S. Li, and M. Chapman, Road surface monitoring using smartphone sensors: A review, *Sensors*, 18(11), DOI: 10.3390/s18113845, 2018.

[4] A. U. Mahin, S. N. Islam, F. Ahmed, and H. F. Hossain, Measurement and monitoring of overhead transmission line sag in smart gird: A review, *IET Generation, Transmission & Distribution*, 16(1), 1-18, 2022.

[5] N. V. S. Korlapati, F. Khan, Q. Noor, S. Mirz, and S. Vaddiraju, Review and analysis of pipeline leak detection methods, *Journal of pipeline science and engineering*, 2(4), 100074, DOI: 10.1016/j.jpse.2022.100074, 2022.

[6] S. Takata, S. Kubota, and N. Watanabe, Prototyping of vibration-sensing-actuation device to realization of future intelligent infrastructure, *Journal of Advanced Mechanical Design, Systems and Manufacturing*, 17(4), DOI: 10.1299/jamdsm.2023jamdsm0045, 2023.

[7] N. Watanabe, and S. Takata, Proposal of control and signal processing method for realization of pipe inspection system based on ring mode of forced vibration, *Proceedings of 2022 JSME-IIP/ASME-ISPS Joint International Conference on Micromechatronics for Information and Precision Equipment (MIPE2022)*, D3-3-03, Nagoya, Japan, 2022.

[8] S. Kubota, and S. Takata, Development of high-power vibration actuator systems for water pipe diagnosis, *Proceedings of 9th International Conference on Manufacturing, Machine Design and Tribology (ICMDT 2023)*, ThA2-2, Jeju, South Korea, 2023.

[9] S. Takata, S. Kubota, and K. Toyoshima, Prototyping of vibration-sensing-actuation device which is contained high-power electrodynamic speaker for diagnosis of actual water main network, INTER-NOISE and NOISE-CON Congress and Conference Proceedings, 270(5) 6500-6508, Nantes, France, DOI: 10.3397/in_2024_3773, 2024.

[10] N. Watanabe, and S. Takata, Proposal of simplified discrimination method for pipe inspection using vibration sensing actuation device, *Proceedings of 9th International Conference on Manufacturing, Machine Design and Tribology (ICMDT 2023)*, ThA2-1, Jeju, South Korea, 2023.

[11] N. Watanabe, and S. Takata, Simplified discrimination method and systematically threshold setting for pipe inspection using vibration-sensing-actuation device, *Journal of Advanced Mechanical Design, Systems and Manufacturing*, 18(1), DOI: 10.1299/jamdsm.2024jamdsm0005, 2024.

[12] X. Liao, Q. Yan, L. Su, Y. Qiu, J. Ren, and C, Zhang, Automatic assesment of freeze-thaw damage in concrete structures using piezoeletric-based active sensing approach and deep learning technique, *Engineering Structures*, 302, 117453, DOI: 10.1016/j.engstruct.2024.117453, 2024.

[13] J. N. Eiras, L. Gaverina, and J-M. Roche, Durability assessment of bonded piezoelectric wafer active seonsor for aircraft health monitoring applications, *Sensors*, 24(450), DOI: 10.3390/s24020450, 2024.

[14] H. Nishikawa, Application of 1D-CAE to the resonance problem of drive system in multifunction printer systems, *Journal of the Imaging Society of Japan*, 59(5), 536-540, 2020 (in Japanese).

[15] M. Inui, and T. Fujinuma, Study of efficient development of 1D CAE models of mechano-electrical products, *Proceedings of the 13th International Modelica Conference*, Regensburg, Germany, DOI: 10.3384/ecp19157751, 2019.

[16] V. Ganesh, Z. He, and W. Zuo, Advancements in building-to-grid interactions: thermos-electric coupling models of motor-driven devices, *Proceedings of the American modelica conference 2024*, DOI: 10.3384/ECP207141, 2024.

[17] S. Borgia, and F. Topputo, Multiphysics acausal modeling and simulation of satellites using modelica library, *Proceedings of the American modelica conference 2024*, DOI: 10.3384/ECP207157, 2024.